Bright Luminescence from Indirect and Strongly Bound Excitons in h-BN

Léonard Schué,[1,2] Lorenzo Sponza,[1] Alexandre Plaud,[1,2] Hakima Bensalah,[2] Kenji Watanabe,[3] Takashi Taniguchi,[3] François Ducastelle,[1] Annick Loiseau,[1,*] and Julien Barjon[2,†]

[1]*Laboratoire d'Etude des Microstructures, ONERA-CNRS, Université Paris-Saclay, BP 72, 92322 Châtillon Cedex, France*

[2]*Groupe d'Etude de la Matière Condensée, UVSQ-CNRS, Université Paris-Saclay, 45 avenue des Etats-Unis, 78035 Versailles Cedex, France*

[3]*National Institute for Materials Science, 1-1 Namiki, Tsukuba 305-0044, Japan*

(Received 12 March 2018; revised manuscript received 28 July 2018; published 12 February 2019)

A quantitative analysis of the excitonic luminescence efficiency in hexagonal boron nitride (h-BN) is carried out by cathodoluminescence in the ultraviolet range and compared with zinc oxide and diamond single crystals. A high quantum yield value of ~50% is found for h-BN at 10 K comparable to that of direct band-gap semiconductors. This bright luminescence at 215 nm remains stable up to room temperature, evidencing the strongly bound character of excitons in bulk h-BN. *Ab initio* calculations of the exciton dispersion confirm the indirect nature of the lowest-energy exciton whose binding energy is found equal to 300 ± 50 meV, in agreement with the thermal stability observed in luminescence. The direct exciton is found at a higher energy but very close to the indirect one, which solves the long debated Stokes shift in bulk h-BN.

DOI: 10.1103/PhysRevLett.122.067401

Hexagonal boron nitride (h-BN) is a wide band-gap semiconductor (> 6 eV) that has recently encountered a tremendous regaining of interest with the emergence of the two-dimensional (2D) crystals family [1,2]. Because of its lattice isostructural to graphene and its excellent dielectric properties, it has been designated as the best insulating material for improving electron mobility in graphene [3] or enhancing intrinsic optical properties of transition metal dichalcogenides (TMDs) [4,5].

In the past decade, the growth of high quality h-BN single crystals has also opened new possibilities for light-emitting devices. Pioneering works by Watanabe *et al.* have revealed the high UV radiative efficiency of h-BN at room temperature [6] and have led to the design of the first h-BN-based light emission device in the deep ultraviolet range [7]. However, the physical mechanisms behind h-BN luminescence are still debated. The main controversy revolves around two apparently contradictory aspects: on the one hand, the highly efficient luminescence (up to 10^3 times higher than in diamond at 300 K) and on the other hand, the energy shift between absorption and emission (Stokes shift).

Among the various interpretations proposed in the past, Watanabe *et al.* first came to the conclusion that h-BN luminescence was driven by direct excitonic recombinations [6], and they attributed the Stokes shift to the lifted degeneracy of free exciton levels due to a dynamical lattice distortion [8]. But recently, Cassabois *et al.* attributed the luminescence lines to phonon-assisted transitions from an indirect exciton [9]. The interpretation is based on a weakly bound hydrogenic picture of the exciton, the Wannier-Mott model, whose limits have already been emphasized for excitons in TMD atomic layers [10–12]. It also does not look pertinent in h-BN where *ab initio* calculations predict a direct exciton close to the Frenkel type [13,14].

Until now, although being widely established, the high luminescence efficiency (LE) of h-BN has never been quantitatively investigated. The classical methods using photoluminescence (PL) combined with integrating spheres [15–17] are not adapted for the deep UV range as required for wide band-gap semiconductors such as h-BN.

In this Letter, we report on a quantitative study of the cathodoluminescence (CL) in h-BN compared to two wide band-gap semiconductors, zinc oxide, and diamond. A careful calibration of our detection setup gives access to the absolute CL intensities in the 200–400 nm range. For the first time, low-temperature measurements (10 K), as a function of excitation depth, provide a value of the internal quantum yield (QY) in a bulk h-BN single crystal. Temperature-dependent CL from 10 K up to 300 K further show the high stability of excitons in bulk h-BN compared to diamond, and this attests of their strong binding energy. These findings are found consistent with *ab initio* calculations performed in this work to establish the dispersion of excitons in h-BN. They have encouraged us to revise the fundamental optical properties of excitons in h-BN, marked by a long debated Stokes shift. A consistent picture describing exciton luminescence and absorption energies is proposed.

For h-BN, all measurements were performed on a single crystal provided by the NIMS (Japan), grown at a high pressure high temperature (HPHT) [18], the highest quality

 © 2019 American Physical Society

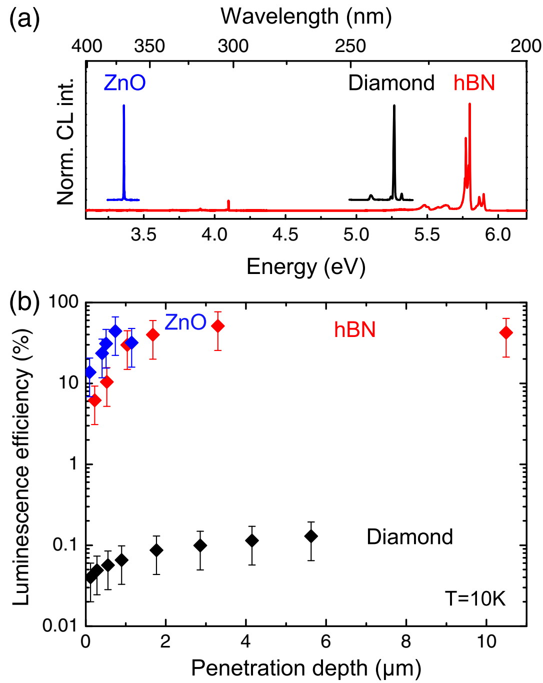

FIG. 1. (a) Cathodoluminescence spectra of h-BN, diamond, and ZnO recorded in the 200–400 nm range at 10 K. For clarity, the excitonic spectra of ZnO and diamond are upshifted. All spectra are corrected from the spectral response of the detection system. (b) Luminescence efficiencies of ZnO, h-BN, and diamond plotted as a function of electron penetration depth. Accelerating voltages from 3 to 30 kV. $T = 10$ K. The incident power Vi is kept constant to avoid nonlinear effects: 1 μW, 6 μW, and 0.4 μW for h-BN, diamond, and ZnO, respectively.

source available today. The diamond and ZnO crystals, as well as the experimental CL set-up, are described in Supplemental Material I [19]. The intensity calibration of the CL detection system relies on a deuterium lamp with a calibrated spectral irradiance (LOT Oriel 30 W) used as a measurement standard within the 200–400 nm wavelength range. Once corrected for the spectral response of the setup, absolute CL intensities are obtained. The light emission power is assessed through a careful evaluation of optical, geometrical, and sample parameters. The full LE measurement procedure, including the absorbed power determination, is detailed in Supplemental Material I. Note that, the uncertainty related to the absolute LE measurements in the deep UV by CL (±50%) is higher than when using integrating spheres in the visible range.

Prior to any quantitative analysis, an overview of the low temperature CL signal is given in the UV range (200–400 nm) for h-BN, diamond, and ZnO single crystals [Fig. 1(a)]. The luminescence of ZnO is dominated by a sharp peak at 3.37 eV, corresponding to the recombinations of neutral-donor bound excitons [34]. In contrast, the luminescence occurs from free excitons in diamond and h-BN. In diamond, it presents a series of lines detected around 5.25 eV coming from phonon-assisted (TA, TO, LO) recombinations of indirect free excitons [35,36]. Similarly, the UV spectrum of h-BN displays a series of sharp lines with a maximum at 5.795 eV, recently attributed to recombinations of indirect free excitons [9]. Note that, in both samples, the luminescence from deep defects is almost undetectable, allowing a proper analysis of the intrinsic excitonic features.

The luminescence efficiencies were measured at increasing accelerating voltages (3–30 kV). In CL, high-energy incident electrons undergo a successive series of elastic and inelastic scattering events in the crystal before being completely stopped. The penetration depth of electrons R_p then increases with the electron beam energy V following the empirical relationship of Kanaya *et al.* [37], $R_p(\mu\mathrm{m}) = C.V(\mathrm{kV})^{1.67}$, where C is a material-dependent parameter.

Figure 1(b) presents the luminescence efficiencies plotted as a function of the penetration depth. While at high R_p, the LE saturates in all cases, and one observes a significant luminescence quenching at low excitation depths. In sp^3 semiconductors such as ZnO or diamond, dangling bonds ending crystal surfaces are known to introduce nonradiative recombination channels that lower the radiative efficiency. In 2D crystals with sp^2 hybridization, dangling bonds are not expected, but the surface effects still remain poorly known. Possible explanations relying on contaminated or defective surface [38] or Auger effects [39] can be invoked to account for this result.

At high penetration depths, the luminescence efficiency reaches a constant value called the internal quantum yield (QY), which is characteristic of the bulk crystal. Generally noted η, it corresponds to the fraction of excitons that recombines radiatively inside the crystal. While the LE most often depends on the crystal orientation, surface terminations, and contaminations, the internal quantum yield remains a reference parameter of the bulk material.

As expected, the direct band-gap ZnO crystal is found to be highly radiative with a QY larger than 50%, in good agreement with previous PL analysis [40]. Conversely, the internal quantum yield of diamond remains close to 0.1%, more than two orders of magnitude lower than in ZnO. Indirect excitons formed in diamond require the simultaneous emission of a phonon to recombine radiatively, which inevitably lowers the probability of such a process. In the case of h-BN, the LE also saturates at high penetration depths but it reaches an ~50% internal quantum yield, comparable to that of a direct semiconductor such as ZnO. Such a high QY value from phonon-assisted recombinations of indirect excitons far exceeds what is commonly observed for indirect semiconductors. It indicates that the nonradiative channels present in the crystal are efficiently bypassed by faster radiative recombinations (a few hundred picoseconds according to the literature [41]).

We then performed temperature-dependence measurements of the luminescence efficiency. Figure 2 first presents

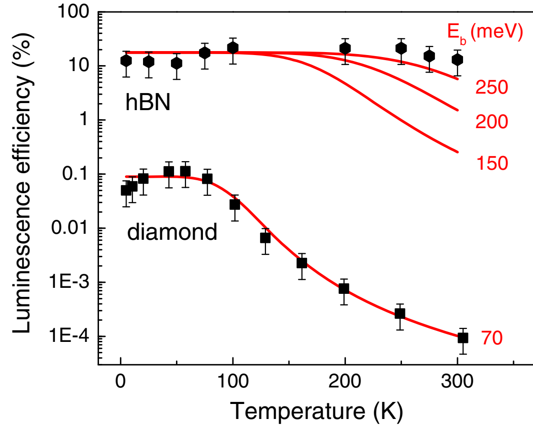

FIG. 2. Luminescence efficiency (logarithmic scale) of h-BN and diamond as a function of temperature. Excitation parameters: $V = 10$ kV, $i = 0.2$ nA for h-BN and 9.5 nA for diamond. The curves (red lines) correspond to the thermal dissociation of excitons (See Supplemental Material II) where E_b is the exciton binding energy.

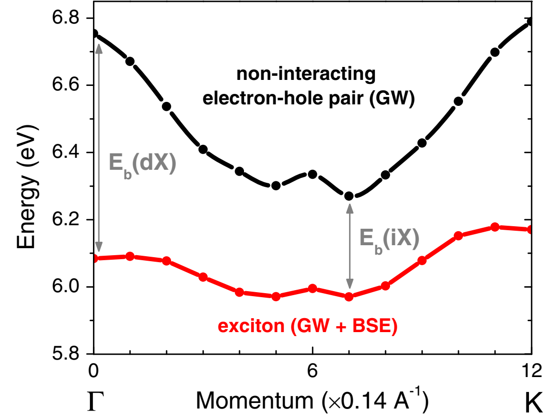

FIG. 3. Dispersion of excitons in h-BN compared to the noninteracting electron-hole pair along the ΓK direction. The vertical arrows indicate the binding energy E_b for the direct (dX) and indirect (iX) excitons. Adapted from Ref. [45].

the CL results obtained on the two indirect band-gap semiconductors, namely h-BN and diamond from 10 to 300 K. To limit surface effects, the accelerating voltage was set at 10 kV. In diamond, the QY is rather stable at low temperatures because of the predominance of the exciton population over free electrons and holes. Above 60 K, the thermal dissociation of excitons occurs and the quasiequilibrium between exciton and free carrier populations is displaced in favor of free carriers, resulting in a drastic LE drop of 3 orders of magnitude. This temperature behavior is well described by the classical model for exciton dissociation in silicon [27,28] recently implemented in diamond [29], with $E_b = 70$ meV in agreement with the reference values of the literature [42,43].

The situation is much different in h-BN, where the LE remains almost constant over the full temperature range. At 300 K, the exciton population is still predominate, demonstrating that the exciton binding energy in h-BN is much higher than in diamond. By applying the same thermal dissociation model (see Supplemental Material II), the binding energy of the lowest-energy excitons in bulk h-BN is estimated to be larger than 250 meV. This lower bound is much higher than the previously reported values in the literature (149 meV [6] and 128 meV [9]).

To elucidate this controversy, the *ab initio* Bethe-Salpeter equation (BSE) has been solved to obtain the exciton dispersion $E_{\rm exc}(Q)$, with Q being the exciton momentum. Quasiparticle energies have been computed within the perturbative *GW* method and further blue shifted by 0.47 eV on the basis of recent electron energy loss spectroscopy experiments [44]. The state-dependent corrections of *GW* ensure an accurate dispersion at the single-particle level. Details of the computational method are given in Supplemental Material III. Two different two-particle dispersion relations can then be obtained. First, the dispersion of the noninteracting electron-hole pair (*GW*, black curve) has been traced by reporting the lowest energy difference between the empty and occupied quasiparticle states compatible with the given $Q = K_e + K_h$. Second, the exciton dispersion (*GW*-BSE, red curve) results from the solution of the BSE at finite Q. Electron-hole pairs formed with electrons sitting in M at the bottom of the conduction band and holes sitting near K at the top of the valence band are expected to have a momentum close to KM = 1/2 ΓK [9]. That is why we report in Fig. 3 both noninteracting *e-h* pair and exciton dispersions along the ΓK direction.

The independent *e-h* dispersion (*GW* curve) reaches its lowest energy near the middle of Γ*K* and lies 0.5 eV below the direct transition (Γ), consistently with the indirect electron band structure (see Supplemental Material III and Ref. [14]). In the presence of Coulombic interactions, the minimum of the exciton energy (*GW*-BSE curve) is also found close to the middle of ΓK at 5.97 eV. The exciton dispersion behavior corroborates the attribution of the luminescence lines as being phonon-assisted recombinations of an indirect exciton [9]. It is also confirmed through high-resolution CL spectroscopy presented in Supplemental Material I. The value of 5.956 eV is found by CL for the no phonon recombination, which accurately defines the indirect exciton (iX) energy in h-BN.

More insights come from the comparison of the exciton and free electron-hole pair dispersions (Fig. 3). Strikingly, excitonic effects tend to flatten the dispersion of the noninteracting electron-hole pair. In other terms, the exciton is found to be much heavier than the sum of the electron and hole masses, a sum that is assumed to be the exciton mass in the Wannier-Mott model. As a first consequence, the binding energies of direct and indirect excitons are different. The binding energy of the indirect

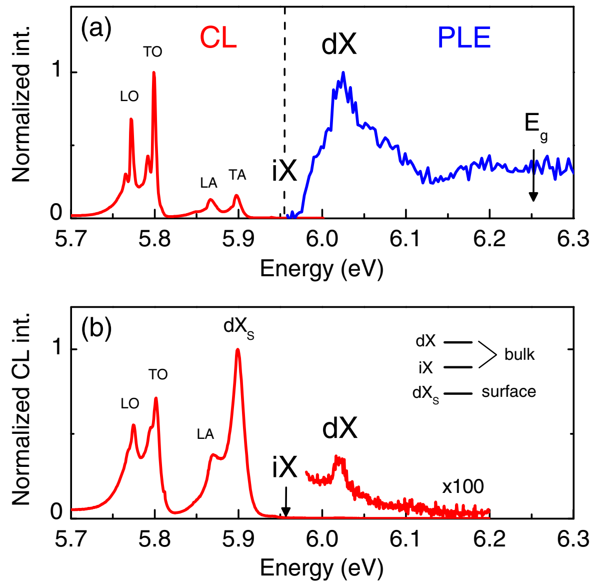

FIG. 4. (a) Normalized spectra of CL and PLE recorded at the CL maximum (from Ref. [46]) illustrating the Stokes shift observed in bulk h-BN crystals. (b) CL spectrum of a thin exfoliated h-BN flake showing the radiative recombination of nonthermalized direct excitons detected at 6.03 eV. CL and PLE spectra taken at 10 K.

exciton $[E_b(iX)]$ is found equal to 300 ± 50 meV (at $Q = (7/12)\Gamma K$), consistent with the high thermal stability observed experimentally (Fig. 2). Incidentally, from the energies found for $E_b(iX)$ and iX, the indirect band-gap energy in bulk h-BN is refined to $E_g = 6.25 \pm 0.05$ eV. Instead, at $Q = 0$, the direct exciton binding energy $E_b(dX)$ is found to be equal to 670 meV, close to the previously reported values [13,14]). The second consequence of the exciton dispersion flattening is that the direct and indirect excitons are very close in energy. The direct exciton lies only ~100 meV above the indirect one.

This theoretical work sheds a new light on the origin of the Stokes shift reported for h-BN between the maxima of luminescence and absorption energies [6,46], as illustrated in Fig. 4(a), with the CL and photoluminescence excitation (PLE) (from Ref. [46]) spectra recorded on the same crystal. It has been reported that the sharp PLE signal peaking at 6.025 eV would arise from a phonon-assisted process [9]. In indirect semiconductors, one should expect a mirror symmetry between absorption and luminescence around the iX energy position [47], both in energy and intensity. It is, however, not observed in h-BN, and it does not apply to interpreting the absorption spectrum.

On the other hand, Fig. 4(a) shows that the energy difference between the iX and the PLE maximum energies, about 70 meV, is comparable to the theoretical ~100 meV energy difference between direct and indirect excitons (Fig. 3). This lets us propose that the dominant PLE peak arises from the direct exciton labeled dX in Fig. 4(a). $Al_xGa_{1-x}As$ alloys face a similar situation when $x \sim 0.3$ but with weakly-bound excitons ($E_b \sim 5$ meV) [48]. The luminescence of h-BN, which only reveals the lowest energy states, is driven by indirect exciton (iX) recombinations, while in the PLE spectrum, being similar to an absorption one, the direct exciton (dX) is predominate.

Even though high resolution absorption data are still lacking, all available experiments exhibit a main peak around 6.1 eV with a strong absorption coefficient, higher than 10^5 cm^{-1} [49–51]. Such a behavior is typical of optical transitions without phonons (in silicon, for instance, α is higher than 10^5 cm^{-1} at the direct gap edge [52]). Furthermore, recent studies have shown that the absorption spectrum of h-BN multilayers is fairly independent of the number of layers [53,54]. The direct exciton is theoretically described as being quite similar in bulk h-BN and in the monolayer, with its energy being weakly influenced by the surrounding BN planes [55–57].

Finally, CL experiments done on exfoliated h-BN samples have also provided precious information. Figure 4(b) displays a typical CL spectrum recorded on an 80 nm thick h-BN flake, where the bulk contribution of indirect excitons (TO, LO, LA, and ZA phonon-assisted lines according to the assignments proposed in Ref. [9]) is detected together with a sharp peak at 5.90 eV. In a previous work [58], we have already shown that when reducing the thickness, a progressive vanishing of the bulk luminescence lines is accompanied by the emergence of a narrow single emission at this energy. This single emission peak tends to indicate that the associated luminescence process does not involve phonons and originates from a direct optical transition. It is further attributed here to surface excitons (dX_S) with zero momentum and an energy slightly below the indirect exciton of bulk h-BN, according to recent theoretical works [59]. More interestingly for the present discussion, in Fig. 4(b) a weak luminescence peak could be detected at 6.03 eV, the same energy as the PLE maximum. It is attributed to the recombination of nonthermalized (hot) direct excitons (dX) from bulk h-BN, observed simultaneously with the TO, LO, LA replica of the indirect one (iX). Finally, the coexistence of direct and indirect excitons with close energies is confirmed as a key to understanding the luminescence and absorption properties of h-BN.

In summary, the luminescence quantum yield in bulk h-BN is quantitatively estimated to be ~50% as high as in direct band-gap semiconductors such as zinc oxide. *Ab initio* calculations of the excitonic dispersion have been decisive in providing a consistent picture of exciton properties in bulk h-BN. The lowest-energy excitons involved in luminescence are of an indirect nature, with a 300 ± 50 meV binding energy, consistent with the stability of the luminescence intensity observed up to room temperature. The excitonic dispersion has revealed the presence of a direct exciton at a slightly higher energy, responsible for the maximum of absorption in bulk h-BN.

The long-standing debate on the Stokes Shift in bulk h-BN is thus completely elucidated. As a perspective, the extremely high efficiency of the phonon-assisted luminescence in h-BN, unique for an indirect band-gap semiconductor, still needs a better understanding for applications with light emitting devices in the deep UV range.

Christèle Vilar is warmly acknowledged for the technical help on the cathodoluminescence-SEM setup. Authors would like to thank the French National Agency for Research (ANR) for funding this work under the project GoBN (Graphene on Boron Nitride Technology), Grant No. ANR-14-CE08-0018. The research leading to these results has also received funding from the European Union Seventh Framework Program under Grant Agreements No. 696656 GrapheneCore1 and No. 785219 GrapheneCore2. Growth of hexagonal boron nitride crystals was supported by the Elemental Strategy Initiative conducted by the MEXT, Japan and JSPS KAKENHI Grant No. JP15K21722.

---

*annick.loiseau@onera.fr
†julien.barjon@uvsq.fr

[1] K. S. Novoselov, A. K. Geim, S. V. Morozov, D. Jiang, Y. Zhang, S. V. Dubonos, I. V. Grigorieva, and A. A. Firsov, Science **306**, 666 (2004).
[2] F. Xia, H. Wang, D. Xiao, M. Dubey, and A. Ramasubramaniam, Nat. Photonics **8**, 899 (2014).
[3] C. R. Dean, A. F. Young, I. Meric, C. Lee, L. Wang, S. Sorgenfrei, K. Watanabe, T. Taniguchi, P. Kim, K. L. Shepard, and J. Hone, Nat. Nanotechnol. **5**, 722 (2010).
[4] F. Cadiz, E. Courtade, C. Robert, G. Wang, Y. Shen, H. Cai, T. Taniguchi, K. Watanabe, H. Carrere, D. Lagarde, M. Manca, T. Amand, P. Renucci, S. Tongay, X. Marie, and B. Urbaszek, Phys. Rev. X **7**, 021026 (2017).
[5] O. A. Ajayi, J. V. Ardelean, G. D. Shepard, J. Wang, A. Antony, T. Taniguchi, K. Watanabe, T. F. Heinz, S. Strauf, X.-Y. Zhu, and J. C. Hone, 2D Mater. **4**, 031011 (2017).
[6] K. Watanabe, T. Taniguchi, and H. Kanda, Nat. Mater. **3**, 404 (2004).
[7] K. Watanabe, T. Taniguchi, T. Niiyama, K. Miya, and M. Taniguchi, Nat. Photonics **3**, 591 (2009).
[8] K. Watanabe and T. Taniguchi, Phys. Rev. B **79**, 193104 (2009).
[9] G. Cassabois, P. Valvin, and B. Gil, Nat. Photonics **10**, 262 (2016).
[10] D. Y. Qiu, F. H. da Jornada, and S. G. Louie, Phys. Rev. Lett. **111**, 216805 (2013).
[11] A. Chernikov, T. C. Berkelbach, H. M. Hill, A. Rigosi, Y. Li, O. B. Aslan, D. R. Reichman, M. S. Hybertsen, and T. F. Heinz, Phys. Rev. Lett. **113**, 076802 (2014).
[12] G. Wang, A. Chernikov, M. M. Glazov, T. F. Heinz, X. Marie, T. Amand, and B. Urbaszek, Rev. Mod. Phys. **90**, 021001 (2018).
[13] L. Wirtz, A. Marini, M. Grüning, and A. Rubio, arXiv:cond-mat/0508421.
[14] B. Arnaud, S. Lebègue, P. Rabiller, and M. Alouani, Phys. Rev. Lett. **96**, 026402 (2006).
[15] G. A. Crosby and J. N. Demas, J. Phys. Chem. **75**, 991 (1971).
[16] J. A. Jacquez and H. F. Kuppenheim, J. Opt. Soc. Am. **45**, 460 (1955).
[17] W. R. Ware and B. a. Baldwin, J. Chem. Phys. **43**, 1194 (1965).
[18] T. Taniguchi and K. Watanabe, J. Cryst. Growth **303**, 525 (2007).
[19] See Supplemental Material at http://link.aps.org/supplemental/10.1103/PhysRevLett.122.067401 for further information on the samples and the CL setup, description of the luminescence efficiency measurement procedure and the analysis of thermal dissociation of excitons, as well as details regarding the *ab initio* calculations, which includes Refs. [20–33].
[20] L. Schué, I. Stenger, F. Fossard, A. Loiseau, and J. Barjon, 2D Mater. **4**, 015028 (2017).
[21] B. G. Yacobi and D. B. Holt, *Cathodoluminescence Microscopy of Inorganic Solids* (Springer, New York, 1990).
[22] M. Pomorski, E. Berdermann, W. de Boer, A. Furgeri, C. Sander, and J. Morse, Diam. Relat. Mater. **16**, 1066 (2007).
[23] M. Pagel, V. Barbin, P. Blanc, and D. Ohnenstetter, *Cathodoluminescence in Geosciences* (Springer-Verlag, Berlin Heidelberg, 2000).
[24] L. Reimer, *Scanning Electron Microscopy* (Springer-Verlag, Berlin Heidelberg, 1985).
[25] A. Segura, L. Artús, R. Cuscó, T. Taniguchi, G. Cassabois, and B. Gil, Phys. Rev. Mater. **2**, 024001 (2018).
[26] S. Adachi, *Optical Constants of Crystalline and Amorphous Semiconductors* (Springer, New York, 1999).
[27] P. L. Gourley and J. P. Wolfe, Phys. Rev. B **25**, 6338 (1982).
[28] D. Labrie and T. Timusk, Solid State Commun. **53**, 327 (1985).
[29] M. Kozák, F. Trojánek, and P. Malý, Phys. Status Solidi A **211**, 2244 (2014).
[30] N. Naka, H. Morimoto, and I. Akimoto, Phys. Status Solidi A **213**, 2551 (2016).
[31] J. Omachi, T. Suzuki, K. Kato, N. Naka, K. Yoshioka, and M. Kuwata-Gonokami, Phys. Rev. Lett. **111**, 026402 (2013).
[32] V. L. Solozhenko, G. Will, and F. Elf, Solid State Commun. **96**, 1 (1995).
[33] F. Paleari, H. P. C. Miranda, A. Molina-Sánchez, and L. Wirtz, arXiv:1810.08976.
[34] C. F. Klingshirn, B. K. Meyer, A. Waag, A. Hoffmann, and J. Geurts, *Zinc Oxyde, From Fundamental Properties Towards Novel Applications* (Springer, Berlin, Heidelberg, 2010).
[35] P. J. Dean, E. C. Lightowlers, and D. R. Wight, Phys. Rev. **140**, A352 (1965).
[36] J. Barjon, Phys. Status Solidi A **214**, 1700402 (2017).
[37] K. Kanaya and S. Okayama, J. Phys. D **5**, 43 (1972).
[38] M. Amani, D.-H. Lien, D. Kiriya, J. Xiao, A. Azcatl, J. Noh, S. R. Madhvapathy, R. Addou, K. C. Santosh, M. Dubey, K. Cho, R. M. Wallace, S.-C. Lee, J.-H. He, J. W. Ager, X. Zhang, E. Yablonovitch, and A. Javey, Science **350**, 1065 (2015).

[39] S. Mouri, Y. Miyauchi, M. Toh, W. Zhao, G. Eda, and K. Matsuda, Phys. Rev. B **90**, 155449 (2014).

[40] M. Hauser, A. Hepting, R. Hauschild, H. Zhou, J. Fallert, H. Kalt, and C. Klingshirn, Appl. Phys. Lett. **92**, 211105 (2008).

[41] K. Watanabe and T. Taniguchi, Int. J. Appl. Ceram. Technol. **8**, 977 (2011).

[42] C. D. Clark, P. J. Dean, and P. V. Harris, Proc. R. Soc. A **277**, 312 (1964).

[43] P. J. Dean and J. C. Male, Proc. R. Soc. A **277**, 330 (1964).

[44] R. Schuster, C. Habenicht, M. Ahmad, M. Knupfer, and B. Büchner, Phys. Rev. B **97**, 041201(R) (2018).

[45] L. Sponza, H. Amara, C. Attaccalite, F. Ducastelle, and A. Loiseau, Phys. Rev. B **97**, 075121 (2018).

[46] L. Museur, G. Brasse, A. Pierret, S. Maine, B. Attal-Tretout, F. Ducastelle, A. Loiseau, J. Barjon, K. Watanabe, T. Taniguchi, and A. Kanaev, Phys. Status Solidi RRL **5**, 214 (2011).

[47] R. J. Elliott, Phys. Rev. **108**, 1384 (1957).

[48] B. Monemar, K. K. Shih, and G. D. Pettit, J. Appl. Phys. **47**, 2604 (1976).

[49] A. Zunger, A. Katzir, and A. Halperin, Phys. Rev. B **13**, 5560 (1976).

[50] O. Stenzel, J. Hahn, M. Roder, A. Ehrlich, S. Prause, and F. Richter, Phys. Status Solidi A **158**, 281 (1996).

[51] T. Q. P. Vuong, G. Cassabois, P. Valvin, E. Rousseau, A. Summerfield, C. J. Mellor, Y. Cho, T. S. Cheng, J. D. Albar, L. Eaves, C. T. Foxon, P. H. Beton, S. V. Novikov, and B. Gil, 2D Mater. **4**, 021023 (2017).

[52] H. R. Philipp and E. A. Taft, Phys. Rev. **120**, 37 (1960).

[53] C.-J. Kim, L. Brown, M. W. Graham, R. Hovden, R. W. Havener, P. L. McEuen, D. A. Muller, and J. Park, Nano Lett. **13**, 5660 (2013).

[54] Z. Liu, Y. Gong, W. Zhou, L. Ma, J. Yu, J. C. Idrobo, J. Jung, A. H. MacDonald, R. Vajtai, J. Lou, and P. M. Ajayan, Nat. Commun. **4**, 2541 (2013).

[55] L. Wirtz, A. Marini, and A. Rubio, Phys. Rev. Lett. **96**, 126104 (2006).

[56] L. Wirtz and A. Rubio, in *B-C-N Nanotubes and Related Nanostructures* (Springer, New York, 2009), Vol. 6, pp. 105–148.

[57] T. Galvani, F. Paleari, H. P. C. Miranda, A. Molina-Sánchez, L. Wirtz, S. Latil, H. Amara, and F. Ducastelle, Phys. Rev. B **94**, 125303 (2016).

[58] L. Schué, B. Berini, B. Plaçais, F. Ducastelle, J. Barjon, A. Loiseau, and A. Betz, Nanoscale **8**, 6986 (2016).

[59] F. Paleari, T. Galvani, H. Amara, F. Ducastelle, A. Molina-Sánchez, and L. Wirtz, 2D Mater. **5**, 045017 (2018).